Quasilinearity in tetratomic molecules: An ab initio study of the CHNO family

M. Mladenovic, M. Elhiyani, Marius Lewerenz

Quasilinearity in tetratomic molecules: An ab initio study of the CHNO family

Mirjana Mladenović, Mohamed Elhiyani, and Marius Lewerenz

Citation: J. Chem. Phys. **130**, 154109 (2009); doi: 10.1063/1.3111810
View online: http://dx.doi.org/10.1063/1.3111810
View Table of Contents: http://jcp.aip.org/resource/1/JCPSA6/v130/i15
Published by the American Institute of Physics.

Quasilinearity in tetratomic molecules: An *ab initio* study of the CHNO family

Mirjana Mladenović,[a] Mohamed Elhiyani,[b] and Marius Lewerenz[c]
Laboratoire Modélisation et Simulation Multi Echelle, Université Paris-Est, MSME FRE3160 CNRS, 5 bd Descartes, 77454 Marne la Vallée, France

(Received 15 January 2009; accepted 11 March 2009; published online 20 April 2009)

We present coupled-cluster CCSD(T) all electron results for the equilibrium structure of isofulminic acid, HONC, together with results for the barrier to linearity and the energetics for the four most stable members of the CHNO isomer family, obtained for the ground electronic states by means of large correlation consistent basis sets. Minimum energy paths along the angular coordinates reported for these CHNO isomers are combined with the dominant kinetic energy contributions to predict key rovibrational spectroscopic features which are clearly reminiscent of quasilinear behavior in tetratomic molecules. © *2009 American Institute of Physics*. [DOI: 10.1063/1.3111810]

I. INTRODUCTION

The rovibrational motion of polyatomic molecules is commonly studied by means of either the linear-molecule or bent-molecule formalism. In the bent-molecule limit, three Euler angles are required to specify the orientation of the body-fixed x,y,z axes, whereas two Euler angles are sufficient in the linear-molecule case. In the bent-linear transition, the rotational degree of freedom of a bent molecule, describing the orbiting about the molecular z axis (a-type rotation), is transformed into a vibrational degree of freedom of a linear molecule. In a near symmetric top for the (harmonic oscillator+rigid rotor) model, the energy levels for the bending vibration and a rotation are given by $\hbar\omega_b(v_b+1/2)+AK_a^2$ for a bent molecule and by $\hbar\omega_{\mathrm{lin}}(v_{\mathrm{lin}}+1)$ for a linear molecule. Whereas any K_a excitation may in principle accompany the bending states of a bent molecule, the rovibrational states of a linear molecule are subject to several restrictions. The two-dimensional bending vibration of a linear molecule possesses the vibrational angular momentum $\hat{l}$ with the allowed quantum number values l given by $v_{\mathrm{lin}},v_{\mathrm{lin}}-2,v_{\mathrm{lin}}-4,\ldots,-v_{\mathrm{lin}}$ (i.e., v_{lin} and l are both even or both odd). Due to angular momentum conservation, $\hat{l}_z=\hat{J}_z$ additionally holds, where J is the overall rotation, such that, e.g., the state $(v_{\mathrm{lin}},l=1)$ becomes accessible only for $J\geq 1$. Consequently, bent molecules and linear molecules possess different rovibrational energy level patterns.

The energy of the first $K_a=1$ (i.e., $l=1$) state is A and $\hbar\omega_{\mathrm{lin}}$ above the ground state in the bent molecule and linear-molecule description, respectively, whereas we have $\hbar\omega_b$ and $2\hbar\omega_{\mathrm{lin}}$ for the first excited $K_a=0$ (i.e., $l=0$) states. To quantify the different molecular classes, Yamada and Winnewisser[1] introduced the following parameter:

$$\gamma_0 = 1 - 4\Delta E_1/\Delta E_0, \tag{1}$$

where ΔE_1 and ΔE_0 stand for the transition energies of the first excited $K_a=1$ and $K_a=0$ states, respectively. The parameter γ_0 assumes a value of -1 in the linear case and 1 in the bent case (since $A\ll\hbar\omega_b$ for typical bent molecules).

Molecules falling between the two limiting cases of typical linear and typical bent molecules are commonly termed quasilinear (or quasibent).[2] The γ_0 values of these molecules are different from ± 1, like, e.g., γ_0 values of -0.65 and $+0.85$ found for HCNO and HNCO,[1] respectively, or $\gamma_0=-0.12$ found for HCCN.[3] It may be emphasized that the applicability of the linear-molecule convention was explicitly shown for HCCN in Ref. 3 in spite of its nonlinear equilibrium geometry [$\angle(\mathrm{HCC})_e=147°$ and $\angle(\mathrm{CCN})_e=175°$]. Quasilinear molecules possess a large-amplitude bending vibration, which is generally (very) anharmonic and (strongly) coupled with the a-type rotation. Large negative l-type splittings, excessive centrifugal distortions, K_a dependences different from the K_a^2 law, and sometimes also anomalous isotope shifts are some of the distinctive features of quasilinearity.[2]

Our interest in the quasilinearity effect is twofold. Since the distinction between a linear-molecule and bent-molecule behavior is occasionally blurred, our ultimate goal is to study the role of the quasilinear (large-amplitude bending) mode and the molecular a-type rotation and their coupling under the real condition of a vibrating-rotating molecule for different molecular classes. Our initial choices were fulminic acid, HCNO, a textbook example for quasilinear molecules, and isocyanic acid, HNCO, classified as quasibent in Fig. 2 of Ref. 1. Another purpose of our work is due to the large body of rotationally resolved experimental data available for HCNO and HNCO and the lack of corresponding theoretical rovibrational studies. To our knowledge, a single theoretical work of this kind is available in the literature. The MP2 study of Pinnavaia *et al.*[4] was, however, in rather poor agreement with experiment. Our investigation was further ex-

[a]Author to whom correspondence should be addressed. Electronic mail: mladenov@univ-mlv.fr.
[b]Electronic mail: elhiyani@univ-mlv.fr.
[c]Electronic mail: lewerenz@univ-mlv.fr.

tended to include also cyanic acid, HOCN, and isofulminic acid, HONC, which can be related to HNCO and HCNO, respectively, by hydrogen migration.

Theoretical studies of quasilinear-molecular systems pose a challenging task due to their complicated rovibrational behavior. To illuminate relevant spectroscopic and dynamic properties by theoretical means, we need full-dimensional rovibrational calculations involving no dynamical approximation in combination with an analytical high-quality potential energy hypersurface. A mandatory initial step of such a study is the identification of a strategy for electronic structure computations, which combines sufficient accuracy with reasonable computational cost. Our present work is a further step in this direction.

A. The CHNO isomer family

The CHNO isomers, containing the four primary elements of organic matter, have been intriguing chemists since the 16th century as described in more detail in the overview by Teles *et al.*[5] Among the numerous arrangements of the four atoms [C,H,N,O], including 24 sequentially bonded forms, only four isomers were found to be stable.[4,6,7] The most stable one, isocyanic acid, HNCO, is energetically followed by cyanic acid, HOCN, fulminic acid, HCNO, and isofulminic acid, HONC. These four isomers possess planar equilibrium structures of *trans* type.[4,7,8]

In experimental studies, isocyanic acid and fulminic acid were for a long time the only representatives of the CHNO family. A low-temperature matrix isolation experiment of Jacox and Milligan[9] provided the first experimental evidence for cyanic acid, showing that irradiation of HNCO produces HOCN. Note that rare gas (Ne, Ar) matrix studies by Bondybey *et al.*[10] found that irradiation of matrix isolated HCNO also produces HOCN. Maier *et al.*[11] claimed to have observed the infrared matrix spectrum of HONC in argon at 12 K. However, these results were later withdrawn in a rarely cited paper[12] entitled "Isofulminic acid-phantom or reality?," with the conclusion that "the generation of this compound remains a challenge." Whereas HNCO and HCNO were extensively studied experimentally by high resolution spectroscopy,[2,13–19] only a few rotational transitions were detected for HOCN (Refs. 20 and 21) and only very recently for HONC (Ref. 22) in a microwave search assisted by unpublished data from the present work.

Regarding previous theoretical work dealing with the CHNO family, we refer to Refs. 5, 8, and 23 for an overview and only mention here theoretical studies including some work on HONC. Poppinger *et al.*[6] and McLean *et al.*[7] identified HONC as a candidate for interstellar (radio) search. Pinnavaia *et al.*[4] reported MP2/TZ2P quadratic and MP2/DZP cubic internal coordinate force field constants, used to derive spectroscopic parameters of HONC by means of a perturbational approach. Mebel *et al.*[24] obtained the geometrical parameters of HONC optimized at the B3LYP/6-311G(d,p) level, as part of their density functional study of CHNO in singlet and triplet electronic states. Schuurman *et al.*[8] reported a frozen-core focal-point analysis for the energetics of the CHNO family, providing the equilibrium geometry of HONC at the CCSD(T)/cc-pVQZ level.

In our recent work,[23] the structural parameters and energetics of the three isomers HNCO, HOCN, and HCNO were analyzed in significant detail. There we showed the importance of including all electrons in the correlation treatment to obtain a converged molecular structure for the extremely floppy HCNO molecule and the correct energetics of the three isomers. As a continuation of this work, we investigated the effect of the augmentation of the standard cc-p(C)VXZ basis set families by diffuse functions. As these calculations progressed, it became clear that there were some interesting features, which invited further study, particularly concerning the equilibrium structure and the energetics of the CHNO family. In this connection, we also extend our work by extensive calculations for isofulminic acid, HONC, in order to refine its structure and to assist future high resolution spectroscopic studies of this species. In addition to the geometrical parameters of HONC, we also provide new information about the CHNO family, in particular, on their angular modes. The latter point is relevant for deeper insight into the nature of quasilinear molecules, for which HNCO and most prominently HCNO are important representatives.[2,25]

In our work, correlation effects are included by means of the coupled-cluster CCSD(T) singles and doubles theory, which includes the effect of connected triple substitutions through perturbation theory (Sec. II). A systematic basis set convergence study with Dunning's correlation consistent basis sets, including several extrapolation schemes, is undertaken first for HONC (Sec. III). The effect of the augmentation of the standard basis set series is investigated for the four most stable CHNO members (Sec. IV). In addition to the exploration of the sensitivity of the structural parameters to the basis set quality and electron correlation, we also continue our effort to develop a qualitative understanding of the angular degrees of freedom of all four molecules (Sec. V).

II. COMPUTATIONAL DETAILS

The electronic structure computations have been carried out by means of the coupled-cluster CCSD(T) method with full iterative treatment of single and double excitations and a perturbative correction for triple substitutions,[26,27] employing Gaussian basis sets. The initial calculations for HONC were performed using Dunning's correlation consistent polarized valence cc-pVXZ ($X=2-6$) and core-valence cc-pCVXZ ($X=2-5$) basis sets,[28,29] as in our previous work on HNCO, HOCN, and HCNO.[23]

To test the description of the outer-valence region, we additionally investigated augmented basis sets[30] of the type aug-cc-pVXZ ($X=2-5$), d-aug-cc-pVXZ ($X=2-5$), and aug-cc-pCVXZ ($X=2-5$). The singly augmented aug-cc-pVXZ and doubly augmented d-aug-cc-pVXZ correlation consistent sets of basis functions were originally constructed by extending the standard cc-pVXZ set by, respectively, one and two supplementary diffuse functions of each angular momentum. The augmented correlation consistent core-valence basis set family, aug-cc-pCVXZ, was developed in a similar fashion from the respective cc-pCVXZ set. For the CHNO isomers,

TABLE I. Basis set dependence and infinite basis extrapolation results for structural parameters (in a_0 and degrees), total energies $E_{\min}$ and E_{lin}, and barrier heights to linearity E_{bar} calculated at the CCSD(T) level of theory for isofulminic acid, HONC.

Planar HONC	r_e(HO)	r_e(ON)	r_e(NC)	$\angle(\text{HON})_e$	$\angle(\text{ONC})_e$	$E_{\min}/E_h$
cc-pVTZ	1.8284	2.5284	2.2324	104.26	172.60	−168.301 160
cc-pVQZ	1.8252	2.5200	2.2247	104.59	172.48	−168.350 833
cc-pV5Z	1.8253	2.5185	2.2233	104.71	172.43	−168.366 708
cc-pV6Z	1.8255	2.5178	2.2229	104.74	172.41	−168.372 266
cc-pCVTZ(all)	1.8263	2.5225	2.2257	104.35	172.65	−168.463 745
cc-pCVQZ(all)	1.8238	2.5140	2.2191	104.74	172.59	−168.524 215
cc-pCV5Z(all)	1.8236	2.5126	2.2176	104.86	172.61	−168.542 901
cc-pCV∞Z (all)	1.8236	2.5120	2.2172	104.91	172.59	
aug-cc-pCVTZ(all)	1.8297	2.5245	2.2269	104.62	172.16	−168.475 247
aug-cc-pCVQZ(all)	1.8251	2.5149	2.2197	104.84	172.37	−168.528 681
aug-cc-pCV5Z(all)	1.8240	2.5131	2.2179	104.89	172.51	−168.544 725
aug-cc-pCV∞Z (all)	1.8237	2.5122	2.2173	104.93	172.52	
Linear HONC	r_e(HO)	r_e(ON)	r_e(NC)	E_{lin}/E_h	$E_{\text{bar}}/\text{cm}^{-1}$	
cc-pVTZ	1.7890	2.3947	2.2371	−168.222 155	17 340	
cc-pVQZ	1.7881	2.3901	2.2291	−168.273 332	17 010	
cc-pV5Z	1.7891	2.3895	2.2276	−168.289 741	16 892	
cc-pV6Z	1.7896	2.3991	2.2272	−168.295 489	16 851	
cc-pCVTZ(all)	1.7871	2.3899	2.2304	−168.385 225	17 233	
cc-pCVQZ(all)	1.7867	2.3855	2.2234	−168.447 301	16 881	
cc-pCV5Z(all)	1.7875	2.3848	2.2217	−168.466 581	16 750	
cc-pCV∞Z (all)		2.3847	2.2212			
aug-cc-pCVTZ(all)	1.7926	2.3930	2.2313	−168.398 120	16 927	
aug-cc-pCVQZ(all)	1.7890	2.3871	2.2239	−168.452 313	16 761	
aug-cc-pCV5Z(all)	1.7884	2.3855	2.2221	−168.468 551	16 718	
aug-cc-pCV∞Z (all)	1.7883	2.3849	2.2215			

the cc-pV5Z, cc-pCV5Z, aug-cc-pV5Z, d-aug-cc-pV5Z, and aug-cc-pCV5Z basis sets of quintuple ζ quality contain 328, 490, 461, 594, and 623 contracted Gaussian-type orbitals, respectively.

For planar HONC and linear HCNO, numerical instabilities were, however, encountered in the calculations employing the d-aug-cc-pV5Z basis set. One may note that a similar situation was also observed in our previous study of the van der Waals complex NH_3-H_2.[31] From the computational point of view, this problem was resolved by combining the d-aug-cc-pVXZ basis for carbon, nitrogen, and oxygen with the aug-cc-pVXZ functions for hydrogen, providing a basis set denoted by d^*-aug-cc-pVXZ here. Since diffuse functions placed on hydrogen are expected not to participate significantly in the outer-valence region, the d^*-aug-cc-pVXZ set is also eligible from the physical point of view. The d^*-aug-cc-pV5Z basis set contains 569 contracted Gaussian-type orbitals for CHNO.

The quality of coupled-cluster results is commonly assessed by means of the T_1 diagnostic,[32] giving the norm of the t_1 amplitude. For HONC, we have obtained T_1 values of approximately 0.014 and 0.017 in all electron correlation and valence electron correlation treatments, respectively. These results indicate a dominant single reference character for HONC.

All electronic structure calculations were done using the MOLPRO package of electronic structure programs.[33] Fully relaxed geometry optimizations were carried out for each of the basis sets by means of numerical derivatives. Harmonic vibrational frequency computations for HONC were performed with numerical derivatives, as implemented in MOLPRO.

In the following text, all electron results are indicated by (all) following a basis set identification, as done before.[23]

III. ISOFULMINIC ACID, HONC

A. Structural parameters

The structural parameters of isofulminic acid as a function of the basis set for the CCSD(T) method are shown in Table I, where $X=3,4,5,6$ stands for triple, quadruple, quintuple, and sextuple ζ polarized valence basis function sets, respectively. The results for both the optimum planar and optimum linear arrangements are summarized there, along with the respective absolute energies $E_{\min}$ and E_{lin} and the height E_{bar} of the barrier to linearity calculated as the linear-bent energy difference, $E_{\text{bar}}=E_{\text{lin}}-E_{\min}$.

Schuurman *et al.*[8] reported the equilibrium geometries $[r_e(\text{HO}), r_e(\text{ON}), r_e(\text{NC}), \angle(\text{HON})_e, \angle(\text{ONC})_e]$ of HONC to be $[1.8251a_0, 2.5173a_0, 2.2227a_0, 104.61°, 172.64°]$ at the

CCSD(T)/cc-pVQZ level in the frozen-core approximation. Whereas good agreement is seen between their results and our CCSD(T)/cc-pVQZ values for r_e(HO) and $\angle$(HON)$_e$, we note differences of $0.0027a_0$, $0.0020a_0$, and 0.16° in the cases of r_e(ON), r_e(NC), and $\angle$(ONC)$_e$, respectively.

The cc-pVXZ basis set family in Table I shows convergence to within $0.0007a_0$ and 0.03° for the bond distances and bond angles at the final cc-pV6Z level in the frozen-core approximation. However, the inclusion of the three 1*s*-like core orbitals located on carbon, nitrogen, and oxygen into the active space of HONC affects the optimum geometry by [$-0.0017a_0$, $-0.0059a_0$, $-0.0057a_0$, +0.15°, +0.18°] at quintuple ζ level, as revealed by a comparison of the cc-pV5Z and cc-pCV5Z(all) results. The augmentation of the cc-pCVXZ set with the diffuse functions increases the bond lengths and the bond angle $\angle$(HON)$_e$ and decreases the heavy atom ONC bending angle. This effect becomes smaller for higher basis set cardinal numbers X. In view of Table I, the more compact cc-pCVQZ(all) basis set appears more efficient in converging $\angle$(ONC)$_e$ and r_e(HO), whereas the more diffuse aug-cc-pCVQZ(all) set is somewhat better for the bending angle HON involving hydrogen. To be noted is an excellent agreement between the optimum geometries determined with cc-pCV5Z(all) and aug-cc-pCV5Z(all), except for the angle $\angle$(ONC)$_e$ for which a deviation of 0.10° is found.

The structural parameters of HONC obtained for the cc-pCVXZ(all) and aug-cc-pCVXZ(all) basis set families at the complete basis set (CBS) limit were estimated with the help of the simple three-parameter exponential form,

$$F(X) = F_\infty + Ae^{-BX}, \tag{2}$$

where F stands for a function to be fitted. The cc-pCV∞Z (all) result for r_e(HO) of linear HONC is not given in Table I due to somewhat nonmonotonic convergence of r_e(HO) within the cc-pCVXZ(all) series.

In Table I, one should note the excellent agreement (within $0.0003a_0$ and 0.07°) between the equilibrium geometrical parameters determined at the cc-pCV∞Z (all) level and in the aug-cc-pCV∞Z (all) approach. In addition, inspection of Table I clearly shows that the $X \to \infty$ situation for $\angle$(ONC)$_e$ is accessed from below in computations with the augmented basis sets, but from above in the nonaugmented case. Based on this observation, the mean value of 172.56° ± 0.05°, obtained from the cc-pCV∞Z (all) and aug-cc-pCV∞Z (all) values, is our best CCSD(T)/(aug-)cc-pCVXZ estimate for the heavy atom ONC bond angle of HONC.

Equilibrium rotational constants calculated from the structural parameters of Table I are collected in Table II for selected basis sets. In these calculations, the atomic masses from Ref. 34 are used for ^{1}H, ^{12}C, ^{14}N, and ^{16}O. The rotational constants derived from the (aug-)cc-pCVXZ(all) structural parameters agree better than 0.02 cm^{-1} with the estimated CBS limits, as seen in Table II. Substituting the recommended value of 172.56° for $\angle$(ONC)$_e$ in combination with the CBS results for the other coordinates, we calculate [A_e, B_e, C_e] of [20.758, 0.370 51, 0.364 01 cm^{-1}] and [20.761, 0.370 45, 0.363 96 cm^{-1}] for planar HONC in the cc-pCV∞Z (all) and aug-cc-pCV∞Z (all) cases, respectively. The latter values should be accurate within 0.003 cm^{-1} (90 MHz) for A_e and 0.000 06 cm^{-1} (2 MHz) for B_e and C_e. One may note that according to Table II, isofulminic acid is a slightly asymmetric prolate top, with a value of $\kappa = -0.9994$ for Ray's asymmetry parameter.

TABLE II. Equilibrium rotational constants A_e, B_e, C_e (in cm^{-1}) for optimum planar HONC and the rotational constant B_{lin} (in cm^{-1}) for optimum linear HONC, calculated using the respective structural parameters reported in Table I.

Basis	A_e	B_e	C_e	B_{lin}
cc-pV6Z	20.643	0.368 83	0.362 36	0.370 04
cc-pCV5Z(all)	20.757	0.370 36	0.363 87	0.371 54
cc-pCV∞Z (all)	20.764	0.370 50	0.364 00	
aug-cc-pCV5Z(all)	20.735	0.370 24	0.363 75	0.371 37
aug-cc-pCV∞Z (all)	20.754	0.370 46	0.363 96	0.371 56

B. Absolute energies

The absolute (total) energy E^∞ of HONC at the CBS limit is estimated for the cc-pCVXZ(all) and aug-cc-pCVXZ(all) basis set families. For these two series, additional calculations for $X=2-4$ were carried out at the respective quintuple ($X=5$) optimum geometries of Table I for both planar and linear HONC. In this fashion, we obtained a data set free of geometry relaxation effect.

Three extrapolation schemes were tested. We first employed the two-step procedure proposed by Helgaker *et al.*,[35] which combines an exponential extrapolation of the Hartree-Fock Self-Consistent Field (SCF) contribution with a $1/X^3$ extrapolation for the correlation contribution,

$$E^{\mathrm{SCF}}(X) = E^{\mathrm{SCF}}_\infty + ae^{-bX}, \tag{3}$$

$$E^{\mathrm{corr}}_{2\mathrm{step}}(X) = E^{\mathrm{corr}}_{\infty,x^3} + c/X^3, \tag{4}$$

such that

$$E^\infty_{2\mathrm{step}} = E^{\mathrm{SCF}}_\infty + E^{\mathrm{corr}}_{\infty,x^3}. \tag{5}$$

The extrapolation strategy of Eq. (5) was compared with the pure exponential fit of the total energy to Eq. (2) for $F=E$, giving a CBS value denoted by E^∞_{exp}. In addition, we also consider the two-exponential approach, in which both the SCF contribution and the correlation contribution are separately fitted to an exponential function, such that

$$E^{\mathrm{corr}}_{\mathrm{exp}}(X) = E^{\mathrm{corr}}_{\infty,\mathrm{exp}} + ce^{-dX}, \tag{6}$$

$$E^\infty_{2\mathrm{exp}} = E^{\mathrm{SCF}}_\infty + E^{\mathrm{corr}}_{\infty,\mathrm{exp}}. \tag{7}$$

We first present the results obtained from $X=2-4$ energy points, computed at the aug-cc-pCVXZ(all) level employing the optimum quintuple geometry. Note that the parameters of $E^{\mathrm{corr}}_{2\mathrm{step}}(X)$ in Eq. (4) were estimated from $X=3$ and 4 only. With the help of Eqs. (2)–(7), we determine values for $E_{2\mathrm{step}}(5)$, $E_{\mathrm{exp}}(5)$, and $E_{2\mathrm{exp}}(5)$ of $-168.546\,689\ E_h$, $-168.544\,540\ E_h$, and $-168.544\,641\ E_h$ for $X=5$, which deviate by $-2.0\times10^{-3}\ E_h$ (-431 cm^{-1}), $1.8\times10^{-4}\ E_h$ (40 cm^{-1}), and $8.4\times10^{-5}\ E_h$ (18 cm^{-1}) from the explicitly

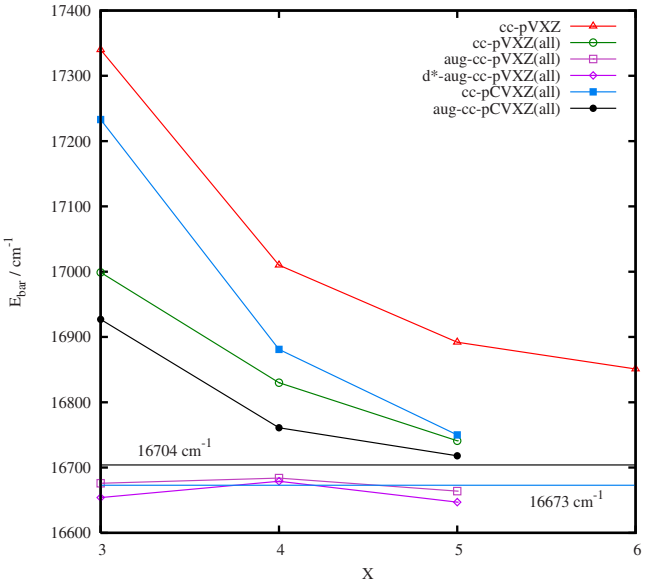

FIG. 1. (Color online) Barrier to linearity of HONC as a function of the cardinal number X of the cc-pVXZ, cc-pCVXZ, aug-cc-pCVXZ, aug-cc-pVXZ, and d^*-aug-cc-pVXZ basis set families.

computed aug-cc-pCV5Z(all) result of −168.544 725 E_h, Table I. Since $E_{2\text{step}}(X)$ and $E_{2\ \text{exp}}(X)$ describe the SCF contribution in the same manner, the large discrepancy found for $E_{2\text{step}}(5)$ clearly indicates that the two-step procedure of Eqs. (3)–(5) overestimates the core correlation contribution in the case of planar HONC. The same effect is also seen for linear HONC.

Using now $X=3-5$ points for the extrapolation, the CBS energies ($E^{\infty}_{\text{min},2\ \text{exp}}$, $E^{\infty}_{\text{lin},2\ \text{exp}}$) estimated for (planar HONC, linear HONC) from the two-exponential extrapolation of Eq. (7) are given by (−168.551 873 E_h, −168.475 758 E_h) for the augmented aug-cc-pCVXZ(all) family and by (−168.551 516 E_h, −168.475 483 E_h) for the cc-pCVXZ(all) series. The corresponding CBS estimates ($E^{\infty}_{\text{min,exp}}$, $E^{\infty}_{\text{lin,exp}}$) obtained from the single exponential extrapolation read (−168.551 599 E_h, −168.475 490 E_h) and (−168.551 247 E_h, −168.475 261 E_h), respectively. For both approaches, the CBS energies for aug-cc-pCVXZ(all) and cc-pCVXZ(all) agree within 0.000 35 E_h (somewhat better for linear HONC).

Since the two-step extrapolation procedure based on Eqs. (3)–(5) showed less satisfactory performance not only in the extrapolations from $X=2-4$ but also from $X=3-5$ data, as well as for the barrier to linearity (Sec. III C), only CBS results obtained from exponential extrapolations are discussed here.

C. Barrier to linearity

The basis set dependence for the height E_{bar} of the barrier to linearity is displayed in Fig. 1. There, E_{bar} clearly decreases upon increasing the cardinal number X due to a somewhat faster lowering of the absolute energy of the linear arrangements as X increases. At the CCSD(T)/cc-pV5Z level, the inclusion of core correlation and the augmentation by diffuse functions lowers the barrier to linearity by 101 and 133 cm^{-1}, see Table I. The structural parameters for the basis set families shown in Fig. 1, but not reported in Table I, can be obtained from the authors by request.

At the quintuple ζ level, the augmented aug-cc-pCV5Z(all) result of Table I for the height E_{bar} of the barrier to linearity is 32 cm^{-1} lower than E_{bar} from the cc-pCV5Z(all) calculations. One should, however, note that E_{bar} in Fig. 1 varies with the cardinal number X somewhat faster for the cc-pCVXZ(all) series than in the aug-cc-pCVXZ(all) case. The single exponential extrapolation of Eq. (2), applied to the $X=3-5$ data of Table I, gives E^{∞}_{bar} values of 16 704 and 16 673 cm^{-1} for the set aug-cc-pCVXZ(all) and cc-pCVXZ(all), respectively. These two results are indicated by the horizontal lines in Fig. 1. In contrast to the $X=5$ situation, E^{∞}_{bar}(cc-pCVXZ) is estimated to be 31 cm^{-1} lower than the augmented CBS result, E^{∞}_{bar}(aug-cc-pCVXZ). For comparison, we also summarize the values $E^{\infty}_{\text{bar},2\ \text{exp}}$ and $E^{\infty}_{\text{bar,exp}}$, which are extrapolated from the $X=3-5$ results for the quintuple optimum geometry. This procedure gives $E^{\infty}_{\text{bar},2\ \text{exp}}$ and $E^{\infty}_{\text{bar,exp}}$ of 16 708 and 16 704 cm^{-1} for aug-cc-pCVXZ(all) and of 16 688 and 16 678 cm^{-1} for cc-pCVXZ(all). Similar results are also obtained from the extrapolated total energies ($E^{\infty}_{\text{min},(2)\text{exp}}$, $E^{\infty}_{\text{lin},(2)\text{exp}}$) of Sec. III B.

With respect to the different extrapolation approaches used here, the CBS results for E_{bar} exhibit rather good convergence within 4 and 15 cm^{-1} for the aug-cc-pCVXZ and cc-pCVXZ series, with, however, different final estimates. In view of Fig. 1, the difference of approximately 30 cm^{-1} between E^{∞}_{bar}(cc-pCVXZ) and E^{∞}_{bar}(aug-cc-pCVXZ) appears somewhat big and is probably due to a core correlation contribution which is overestimated in the extrapolation procedure within the cc-pCVXZ series. To resolve this problem, additional investigations are necessary, including computations with a cc-pCV6Z basis set (currently not available).

TABLE III. Harmonic wavenumbers (in cm^{-1}) of HONC computed at the optimum geometries reported in Table I.

HONC	cc-pVTZ	cc-pVQZ[a]	Normal mode
$\omega_1(a')$	3770	3773	H–O stretch
$\omega_2(a')$	2160	2171	N–C stretch
$\omega_3(a')$	1431	1430	H–O–N bend
$\omega_4(a')$	962	971	O–N stretch
$\omega_5(a')$	249	247	O–N–C bend
$\omega_6(a'')$	303	300	Torsion

[a]The corresponding VQZ(all) results are found to be 3782, 2187, 1431, 978, 255, and 310 cm^{-1}.

D. Harmonic frequencies

Harmonic frequencies, although quantitatively unreliable in a quasilinear system can, however, provide a first insight into the shape of a potential surface and its convergence with respect to the level of calculation. The harmonic wavenumbers of HONC from the CCSD(T)/cc-pVTZ and CCSD(T)/cc-pVQZ calculations are reported in Table III, where the symmetry labels of the C_s point group are used. The ω_i values were evaluated numerically for the respective optimum geometries listed in Table I. Table III shows that the differ-

TABLE IV. Structural parameters (in a_0 and degrees), total energies E_{min} and E_{lin} of optimum planar and optimum linear configurations, and barrier height to linearity $E_{bar}=E_{lin}-E_{min}$ calculated for fulminic acid, HCNO, at the CCSD(T) all electron correlation level of theory using the aug-cc-pCVXZ ($X=2-5$) basis set family.

Planar HCNO	r_e(HC)	r_e(CN)	r_e(NO)	$\angle(\mathrm{HCN})_e$	$\angle(\mathrm{CNO})_e$	E_{min}/E_h
aug-cc-pCVDZ(all)	2.0340	2.2414	2.2953	153.77	173.42	−168.314 416
aug-cc-pCVTZ(all)	2.0054	2.1979	2.2790	173.24	178.40	−168.497 133
Linear HCNO	r_e(HC)	r_e(CN)	r_e(NO)	E_{lin} (E_h)	E_{bar} (cm^{-1})	
aug-cc-pCVDZ(all)	2.0272	2.2240	2.3034	−168.314 416	74.30	
aug-cc-pCVTZ(all)	2.0050	2.1968	2.2796	−168.497 132	0.03	
aug-cc-pCVQZ(all)	2.0026	2.1912	2.2739	−168.551 446		
aug-cc-pCV5Z(all)	2.0020	2.1897	2.2723	−168.567 683		
aug-cc-pCV∞Z (all)	2.0018	2.1891	2.2717			

ence between ω_i values at the CCSD(T)/cc-pVTZ and CCSD(T)/cc-pVQZ levels is at most 11 cm^{-1} and generally much smaller.

The CCSD(T)/cc-pVQZ harmonic wavenumbers of HONC can now be compared with some of the results reported for HCNO, HNCO, and HOCN in Table VII of Ref. 23. First note that the HO stretching frequency ω_1 of 3773 cm^{-1} for HONC is similar to the corresponding value for HOCN, determined to be 3809 cm^{-1}. On the other hand, the CN stretching ω_2 frequency of 2171 cm^{-1} differs by 96 cm^{-1} from the value of 2267 cm^{-1} for HCNO, in contrast to the similar ω_2 results of 2307 and 2325 cm^{-1} found for HNCO and HOCN. Note also that the harmonic wavenumbers of the NO stretch and the ONC bend are approximately 300 cm^{-1} lower in HONC than in HCNO. Finally, the harmonic heavy atom bending wavenumber ω_5 and the harmonic torsional wavenumber ω_6 of isofulminic acid are the lowest among all of the four most stable members of the CHNO family.

Teles *et al.*[5] reported fundamental transitions of HONC at 3443.7, 2190.1, 1232.4, 628.4, 361.2, and 379.3 cm^{-1} in their low-temperature argon matrix study of the CHNO isomers. A comparison of the latter values with the harmonic wavenumbers of Table III shows large deviations not only for ω_1 but also for ω_3 and ω_4. The difference of approximately 350 cm^{-1} seen for the ON stretch ω_4 is very big and raises doubts about the assignment. In this context it is worthwhile mentioning that already Teles *et al.*[5] had some doubts regarding their assignments for ν_3 and ν_4. In 1997, the assignment to isofulminic acid of the experimental infrared spectra observed in Refs. 5 and 11 was entirely withdrawn.[12]

IV. CHNO ISOMERS AT THE CCSD(T)/AUG-CC-PCVXZ LEVEL

Our investigation of HONC with various Dunning-type correlation consistent basis set families clearly shows the most balanced performance for the CCSD(T)/aug-cc-pCVXZ(all) approach which is characterized by monotonic convergence of several quantities studied in Sec. III. We also tested the performance of the CCSD(T) method in conjunction with the augmented bases for the calculation of the other CHNO isomers. In particular, we were interested in HCNO due to previously observed difficulties to arrive at a converged equilibrium geometry for this species.[23]

A. Fulminic acid

Selected results for HCNO are summarized in Table IV. There we collect the geometrical parameters, the total energies, and the height of the barrier to linearity, computed by means of the aug-pCVXZ(all) basis set series, including all electrons in the correlation treatment. Related results from CCSD(T)/cc-p(C)VXZ calculations are given in Table I of Ref. 23.

In our previous work,[23] a small barrier to linearity of 2.19 cm^{-1} was determined for HCNO within the CCSD(T)/cc-pCVQZ(all) approach. The CCSD(T)/cc-pCV5Z(all) equilibrium geometry of HCNO was, however, found to be linear. For the augmented basis function series in Table IV, HCNO possesses a negligible barrier to linearity at the triple ζ level, becoming strictly linear at the quadruple ζ level. In addition, note the excellent agreement (of approximately $0.0006a_0$) between the optimum aug-cc-pCV5Z geometry and the CBS estimate, aug-cc-pCV∞Z (all), obtained from the single exponential extrapolation of Eq. (2).

The cc-pCV5Z(all) equilibrium geometry $[r_e(\mathrm{HC}), r_e(\mathrm{CN}), r_e(\mathrm{NO})]$ was previously reported to be $[2.0017a_0, 2.1896a_0, 2.2713a_0]$.[23] Compared to the aug-cc-pCV5Z(all) results of Table IV, we see that the inclusion of diffuse functions at the quintuple ζ level most prominently affects the bond length r_e(NO), which increases by $0.0010a_0$ upon this basis set augmentation.

The equilibrium rotational constant B_e for HCNO is calculated to be 0.383 52 cm^{-1} (11498 MHz), 0.383 35 cm^{-1} (11492 MHz), and 0.383 56 cm^{-1} (11499 MHz) for the respective optimum cc-pCV5Z(all), aug-cc-pCV5Z(all), and aug-cc-pCV∞Z (all) linear geometries. These three results for B_e agree within 7 MHz. The experimental B_0 value is known to be 0.382 57 cm^{-1} (11 469 MHz).[36]

B. CHNO family

The effect of the improvement of the standard basis set through inclusion of diffuse functions is shown for basis sets of quadruple ζ quality in Table V, where we compare the

TABLE V. Structural parameters (in a_0 and degrees) for optimum planar and linear configurations, barrier height to linearity E_{bar}, and energy Δ measured relative to the respective equilibrium HNCO energy, computed for HNCO, HOCN, HCNO, and HONC at the CCSD(T) all electron correlation level of theory for the cc-pCVQZ and aug-cc-pCVQZ basis sets.

	HNCO		HOCN	
Quantity	cc-pCVQZ(all)	aug-cc-pCVQZ(all)	cc-pCVQZ(all)	aug-cc-pCVQZ(all)
r_e(HX)	1.895 8	1.896 8	1.819 9	1.820 9
r_e(XY)	2.295 5	2.296 5	2.458 1	2.458 3
r_e(YZ)	2.200 0	2.200 8	2.189 8	2.190 7
$\angle(\mathrm{HXY})_e$	123.27	123.45	109.49	109.64
$\angle(\mathrm{XYZ})_e$	172.39	172.33	176.83	176.77
r_e^{lin}(HX)	1.863 9	1.865 0	1.779 5	1.781 0
r_e^{lin}(XY)	2.226 2	2.227 1	2.360 1	2.360 6
r_e^{lin}(YZ)	2.218 8	2.219 7	2.196 5	2.197 4
E/E_h	−168.658 308	−168.662 927	−168.619 465	−168.623 860
E_{bar}/cm^{-1}	1847	1839	9515	9406
Δ/cm^{-1}			8525	8577
	HCNO		HONC	
Quantity	cc-pCVQZ(all)	aug-cc-pCVQZ(all)	cc-pCVQZ(all)	aug-cc-pCVQZ(all)
r_e(HX)	2.003 0		1.823 8	1.825 1
r_e(XY)	2.194 5		2.514 0	2.514 9
r_e(YZ)	2.269 3		2.219 1	2.219 7
$\angle(\mathrm{HXY})_e$	168.76		104.74	104.84
$\angle(\mathrm{XYZ})_e$	177.44		172.59	172.37
r_e^{lin}(HX)	2.001 9	2.002 6	1.786 7	1.789 0
r_e^{lin}(XY)	2.191 6	2.191 2	2.385 5	2.387 1
r_e^{lin}(YZ)	2.270 8	2.273 9	2.223 4	2.223 9
E/E_h	−168.546 525	−168.551 446	−168.524 215	−168.528 681
E_{bar}/cm^{-1}	2.2		16 881	16 761
Δ/cm^{-1}	24 534	24 467	29 430	29 464

structural parameters of HNCO, HOCN, HCNO, and HONC obtained from the CCSD(T)/aug-cc-pCVQZ(all) and CCSD(T)/cc-pCVQZ(all) calculations.

The results of Table V typically show increases in the bond lengths (up to $0.0031a_0$), increases in the bond angle HXY involving hydrogen (up to 0.18°), and decreases in the heavy atom bending angle XYZ (up to 0.22°) upon augmentation by diffuse functions. Note that the bond distances r_e^{lin}(HX), r_e^{lin}(XY), r_e^{lin}(YZ) of the optimum linear configuration are somewhat more affected than the coplanar configuration values. In particular, the bond distances involving oxygen show a high level of sensitivity to the basis set augmentation in Table V.

In addition, Table V also presents the height E_{bar} of the barrier to linearity and the energy Δ measured relative to the respective energy of the most stable isomer, isocyanic acid, HNCO. Upon inclusion of diffuse functions, the barrier to linearity decreases by 8, 109, and 120 cm^{-1} for, respectively, HNCO, HOCN, and HONC, whereas HCNO becomes strictly linear. At the same time, the relative energy Δ increases by 52 and 34 cm^{-1} for HOCN and HONC and decreases by 57 cm^{-1} in HCNO.

V. ANGULAR PATHS FOR THE CHNO ISOMERS

In the internal dynamics of quasilinear molecules, the angular motion plays a major role due to its large-amplitude character, which may lead to prominent radial-angular and rotation-angular couplings. We have thus investigated in some detail the angular features of the potential energy surfaces of the four CHNO isomers by exploring one-dimensional angular paths obtained by optimization of the remaining coordinates at each angle. Since these numerous minimizations are most economically done with modest basis set sizes, we report here the angular paths obtained by means of CCSD(T)/cc-pVQZ(all). The chosen approach should, however, be sufficient for the qualitative understanding of the main angular properties of the CHNO family.

The angular space of a HXYZ molecule is commonly parametrized in terms of two in-plane bending angles, $\angle(\mathrm{HXY})$ and $\angle(\mathrm{XYZ})$, and one dihedral (torsion) angle. The minimum energy paths (MEPs) along these three angular coordinates are displayed in Figs. 2–4 for the CHNO family members. The MEPs in the direction of the bending angles are explored for coplanar atom arrangements. The profiles of Figs. 2–4 clearly show a single minimum well for each of the angular degrees of freedom.

The MEPs in the direction of the bending angle HXY in Fig. 2 possess well depths ranging from 0 (HCNO), over approximately 1800 cm^{-1} for HNCO and approximately 9400 cm^{-1} for HOCN to approximately 16 800 cm^{-1} for HONC. Their common features are a significant angular width and anharmonic shape. The HXY profiles are some-

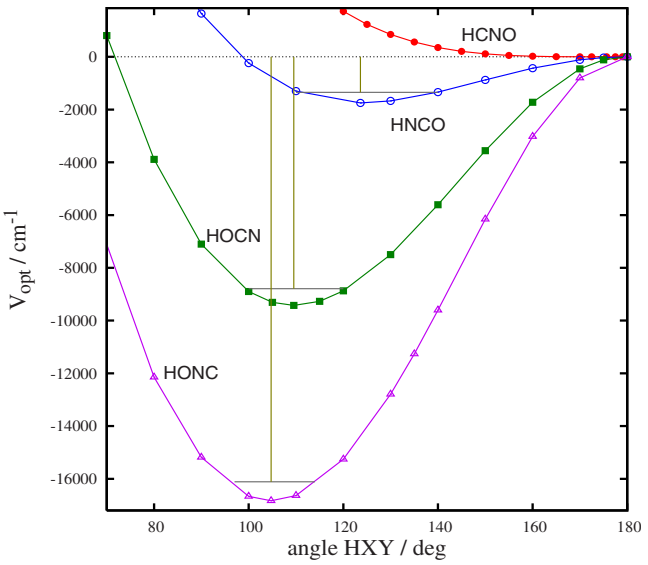

FIG. 2. (Color online) Minimum energy CCSD(t)/cc-pVQZ(all) paths along the bond angle HXY, measured relative to the energy of the respective optimum linear configuration.

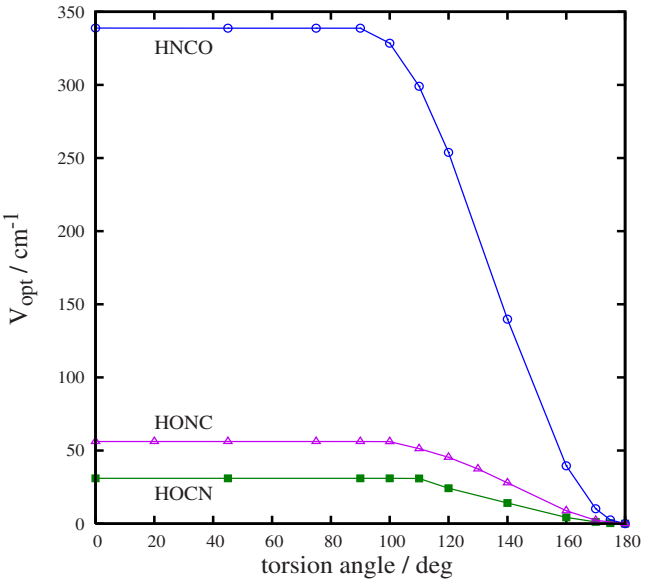

FIG. 4. (Color online) Minimum energy CCSD(t)/cc-pVQZ(all) paths along the torsional angle, measured relative to the energy of the respective optimum equilibrium configuration.

what less steep for HXY angles larger than the equilibrium value $\angle(\mathrm{HXY})_e$, as indicated by the vertical lines drawn in Fig. 2 at the respective equilibrium angle $\angle(\mathrm{HXY})_e$ for HNCO, HOCN, and HONC. The horizontal lines in Fig. 2 give the location of the respective ground state expected in the harmonic approximation, using $\omega(\mathrm{HXY})$ of 805, 1273, and 1431 cm^{-1} for HNCO, HOCN, and HONC (Table III of the present work and Table VII of Ref. 23). As seen, the harmonic ground state wave function explores an angular width of approximately 30° for HNCO and approximately 20° for HOCN and HONC.

Inspection of the changes of the optimum bond distances along the angular paths may provide first insights into the nature of the radial-angular coupling. In Fig. 5, we therefore present the variation of the optimum coordinate triplet $[r_{\mathrm{opt}}(\mathrm{HO}), r_{\mathrm{opt}}(\mathrm{ON}), r_{\mathrm{opt}}(\mathrm{NC})]$ along the MEP in the direction of the HON bond angle of isofulminic acid. The optimum triplet in Fig. 5 is $[1.822a_0, 2.513a_0, 2.219a_0]$ for $\angle(\mathrm{HON}) = 104.7°$ (equilibrium) and $[1.785a_0, 2.385a_0, 2.223a_0]$ for linear $\angle(\mathrm{HON}) = 180°$, corresponding to changes of -0.037, -0.128, and $+0.004a_0$, respectively. Note that the decrease in $r_{\mathrm{opt}}(\mathrm{HX})$ and $r_{\mathrm{opt}}(\mathrm{XY})$ upon straightening of the bending HXY angle was previously observed also for the other three CHNO family members (Fig. 5 of Ref. 23). In addition, since the bond length $r(\mathrm{ON})$ enters the definition of the reduced mass for both the HON and ONC bending vibrations [see Eq. (14) of the next section], the prominent changes of $r_{\mathrm{opt}}(\mathrm{ON})$ in Fig. 5 should also have a pronounced effect on the overall bending dynamics of HONC.

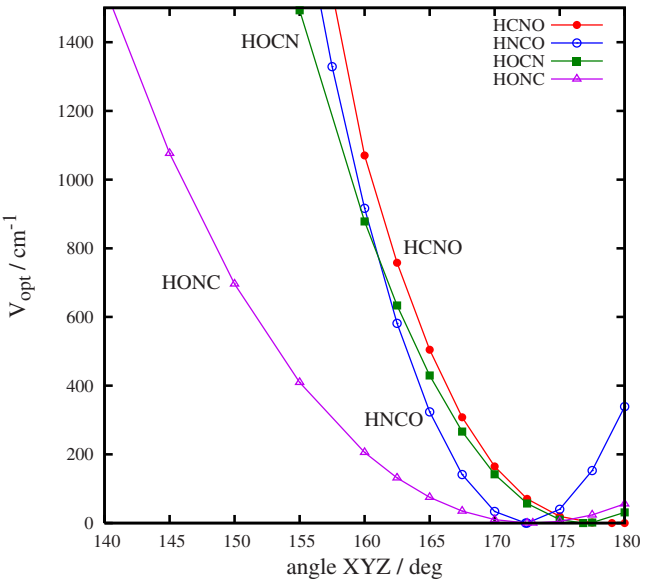

FIG. 3. (Color online) Minimum energy CCSD(t)/cc-pVQZ(all) paths along the bond angle XYZ, measured relative to the energy of the respective optimum equilibrium configuration.

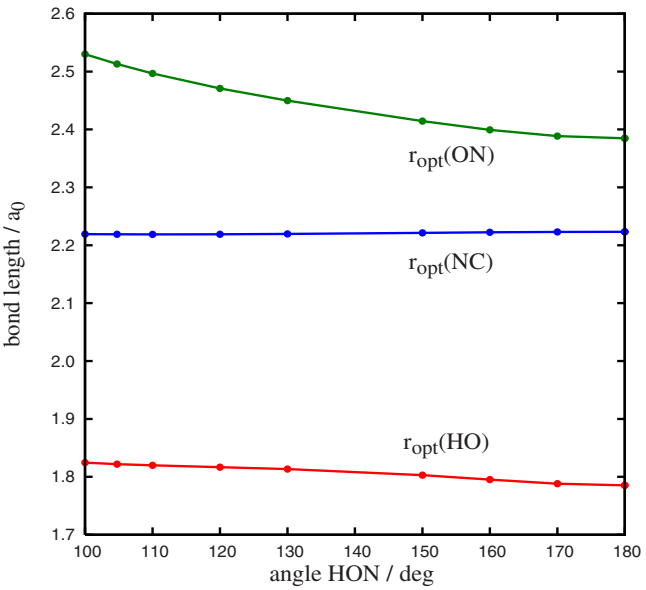

FIG. 5. (Color online) Variation of the optimum bond lengths $r_{\mathrm{opt}}(\mathrm{HO})$, $r_{\mathrm{opt}}(\mathrm{ON})$, and $r_{\mathrm{opt}}(\mathrm{NC})$ along the MEP in the direction of the bending angle HON of isofulminic acid.

TABLE VI. Geometrical parameters (in a_0 and degrees) and the associated total energy E for the hockey-stick structure of HONC at the CCSD(T)/cc-pVQZ(all) level.

Quantity	Value
$r(\mathrm{HO})_e$	1.822 2
$r(\mathrm{ON})_e$	2.513 1
$r(\mathrm{NC})_e$	2.218 3
$\angle(\mathrm{HON})_e$	104.61
$\angle(\mathrm{ONC})_e$	180.0
E/E_h	−168.439 815

Figure 3 shows the MEPs along the heavy atom XYZ bond angle. In the case of HCNO and HNCO, these appear to be somewhat stiffer than the corresponding HXY MEPs of Fig. 2. Among the four XYZ angular profiles, HONC possesses the smallest curvature, leading to the lowest ω(XYZ) wavenumber, as described before. Upon straightening of the XYZ bending angle, the optimum bond lengths r_e(XY) and r_e(YZ) are found to decrease (most prominently in fulminic acid), accompanied by a weak variation of r_e(HX) (on the order of $0.001a_0$). The optimum value for the angle HXY along the XYZ MEP undergoes only small changes (within 1°) for HNCO, HOCN, and HONC. In HCNO, the optimum HCN angle varies in a more pronounced fashion, decreasing from e.g., 180° to 139° when ∠(CNO) changes from 180° to 150°.

The MEPs in the direction of the torsional angle τ are shown in Fig. 4 for HNCO, HOCN, and HONC. Note a single (*trans*) minimum at $\tau=180°$. Since HCNO is linear at the CCSD(T)/cc-pVQZ(all) level (see Table I of Ref. 23), the torsional profile for HCNO is not given here. The three optimum bond distances and the optimum bond angle HXY exhibit only weak changes along the torsional paths of Fig. 4 (on the order of $0.005a_0$ and 0.3°), whereas the heavy atom bending angle XYZ varies from the equilibrium value of 172° –177° at $\tau=180°$ to $\angle(\mathrm{XYZ})=180°$ for $\tau\leq 90-110°$. This straightening of the XYZ subunit, accompanying the decrease in τ, leads to optimum potential energy profiles independent of the torsional angle for $\tau\leq 90°-110°$ (Fig. 4).

Molecular arrangements of HXYZ with a strictly linear heavy atom XYZ skeleton are commonly referred to as "hockey-stick" structures.[37] To complement the optimum hockey-stick data for HNCO, HOCN, and HCNO in Table VI of Ref. 23, we summarize the corresponding results for HONC in Table VI of the present work. The striking similarity of optimum hockey-stick HONC to optimum planar (equilibrium) HONC in Tables VI and I, respectively, is easy to understand in view of the previous discussion of the XYZ and torsional MEPs. Note that the onset of the hockey-stick structure for HNCO, HOCN, and HONC occurs in Figs. 3 and 4 at low energies of 339, 31, and 56 cm^{-1} above the respective global minima.

Substituting the harmonic wavenumbers for the HXY bend and the equilibrium rotational constants A_e (the bent molecule approach) into Eq. (1), the quasilinearity parameter γ_0 is calculated to be 0.86, 0.93, and 0.94 for HNCO, HOCN, and HONC, respectively. The classification of the angular motion due to Yamada and Winnewisser[1] consequently places these molecules rather close to the bent molecule limit. For the heavy atom XYZ bend, we obtain γ_0 values of 0.80, 0.79, and 0.67 for, respectively, HNCO, HOCN, and HONC. Note that full rovibrational calculations are necessary to derive a theoretical γ_0 value for the electronically linear HCNO molecule.

A. Rotational constants

The variation of the optimum rotational constants B_{opt} and C_{opt} along the HXY and XYZ MEPs of Figs. 2 and 3 is shown in Fig. 6, whereas the corresponding variation of the optimum rotational constant A_{opt} is seen in Fig. 7. The purpose of Figs. 6 and 7 is to gain a first insight into the nature of the rotation-angular coupling. The optimum rotational constants A_{opt}, B_{opt}, C_{opt} (where $A\geq B\geq C$) are obtained by

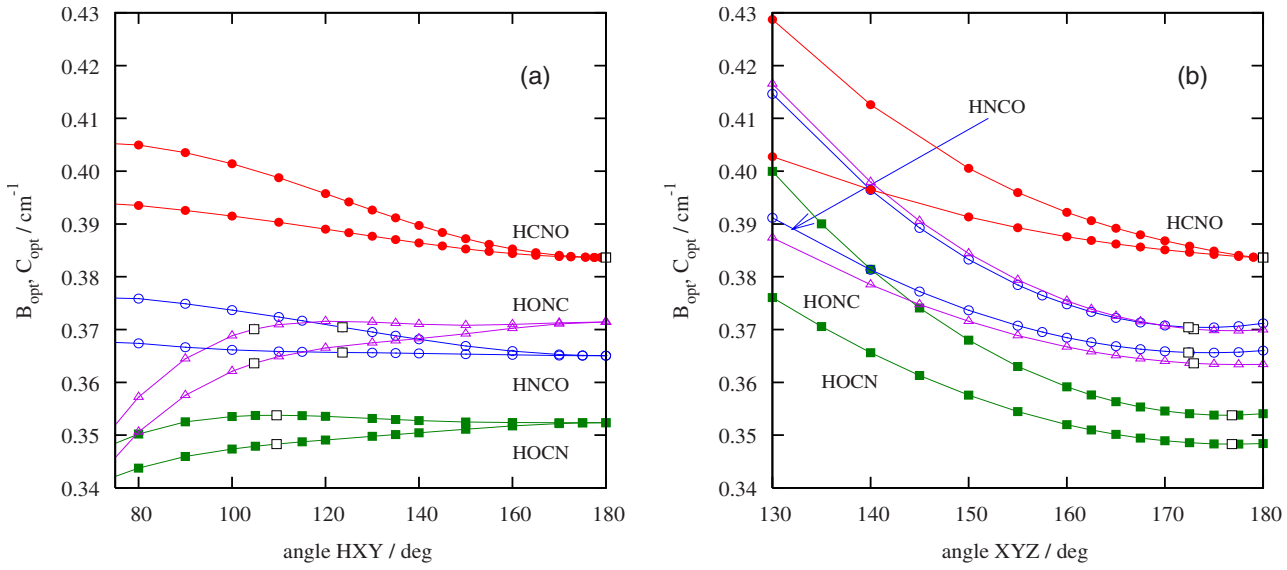

FIG. 6. (Color online) Variation of the optimum rotational constants B_{opt} and C_{opt} for the CHNO family along the MEP in the direction of the bond angle HXY in (a) and in the direction of the heavy atom bond angle XYZ in (b).

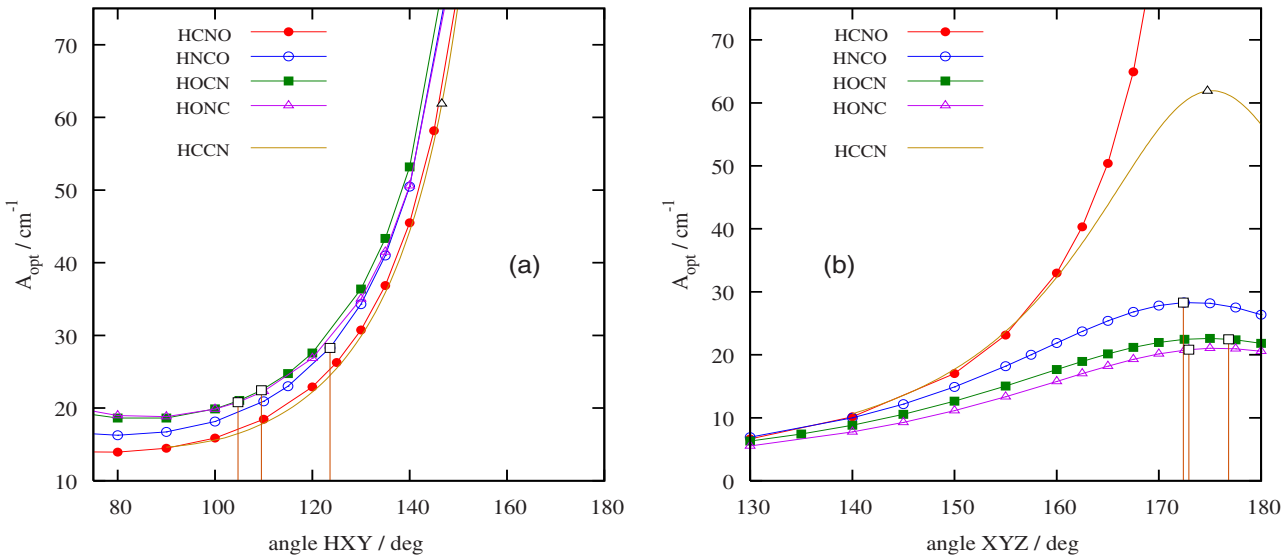

FIG. 7. (Color online) Variation of the optimum rotational constant A_{opt} for the CHNO family and HCCN along the MEP in the direction of the bond angle HXY in (a) and in the direction of the heavy atom bond angle XYZ in (b).

inverting the principal values of the moment-of-inertia tensor, computed along the MEPs. The equilibrium values A_e, B_e, C_e are indicated by the white boxes in Figs. 6 and 7.

The expected increase in B_{opt} and C_{opt}, accompanied by an increase in the difference $B_{opt}-C_{opt}$, upon lowering of the bending angles $\angle$(HXY) and $\angle$(XYZ) is seen for most of the curves shown in Fig. 6. Note, however, a lowering of B_{opt} and C_{opt} along the HXY MEP for HOCN and HONC, which may in principle lead to an unusual vibrational dependence of the respective effective rotational constants of these two species.

The rotational constant A_{opt} along the HXY MEP in Fig. 7(a) grows rapidly to infinity upon straightening of the bond angle $\angle$(HXY) involving hydrogen (the linear-molecule limit). Under these circumstances, the rotation-angular coupling in real vibrating molecules will become particularly important for those vibrational states described by wave functions of considerable extent over close-to-linearity arrangements (in the vicinity and above the barrier to linearity). Such a situation may lead to an effective (vibrationally averaged) rotational constant A_v (much) larger than the equilibrium A_e value. Among the three nonlinear CHNO members in Fig. 7(a), the most pronounced rotational-vibrational coupling is to be expected for HNCO, in qualitative agreement with the large centrifugal distortion D_K constant experimentally found to be 5940 MHz (0.2 cm^{-1}) for HNCO.[38]

Along the HXY MEP of Fig. 7(a), the body-fixed z axis departs from the XY direction by a few degrees (up to approximately 8°) due to a nearly linear heavy atom chain XYZ (see Sec. IV B). Around $\angle$(HXY) of 90°, the rotational constant A_{opt} approaches a value close to the rotational constant of the HX subunit. The latter molecular arrangements with the HX bond oriented perpendicular to the angular momentum vector are accessible in rotating molecules in the high K limit (rotational saturation). In the case of HOCN and HONC, with $\angle(\mathrm{HXY})_e$ of approximately 110° and 105° (Table V), the equilibrium rotational constant A_e is already rather close to $A_{opt}(\angle(\mathrm{HXY})=90°)$. Interpretation of the rotational saturation effect for the heavy atom XYZ bend is less simple, since in addition to hydrogen also the heavy atom(s) bending away from the angular momentum z axis may prominently contribute to the A rotational constant of CHNO.

In K excited states, the vibrational wave function is pushed inward away from the linearity region (by an additional centrifugal potential), such that a lowering of the effective A_v constant may occur upon increasing K for states of the excited in-plane HXY bend, Fig. 7(a). On the other hand, the effective A_v constant for the small-amplitude XYZ mode of HNCO, HOCN, and HONC around $\angle(\mathrm{HXY})_e$ seems to be less sensitive to K excitation, Fig. 7(b). Therefore vibrational states of the rotationally excited HXY bend and vibrational states of the rotationally excited heavy atom XYZ bend are expected to exhibit different K patterns. One may note that this was previously found for cyanocarbene, HCCN, as seen in Fig. 7 of Ref. 3. While the small-amplitude ν_4 (~CCN) bending vibration of HCCN exhibits a typical two-dimensional oscillator structure [described by $E_{v_4}(K_1) \approx E_{v_4}(K_2)$ for allowed K values], $E_{v_5}(K_2) < E_{v_5}(K_1)$ was found for $K_2 > K_1$ for the large-amplitude ν_5 (~HCN) bending vibration [e.g., the level $2\nu_5^2$ lies 118 cm^{-1} below $2\nu_5^0$]. For the purpose of comparison, the optimum rotational constant A_{opt} for HCCN is also displayed in Fig. 7, where the white triangles indicate the equilibrium value A_e(HCCN). Note that A_{opt}(HCNO) closely follows A_{opt}(HCCN) in Fig. 7(a).

For planar tetratomic molecules involving hydrogen attached to a nearly linear heavy atom chain, the behavior of the rotational constant A_{opt} in Fig. 7 is easy to rationalize in qualitative terms with the help of the appropriate element of the moment-of-inertia tensor. As found[39] in Ref. 40, the moment of inertia I_{zz} is given by

$$I_{zz} = \mu_1 d_1^2 \sin^2 \theta_1 + \mu_2 d_2^2 \sin^2 \theta_2 \qquad (8)$$

for tetratomic molecules described by the orthogonal coordinates $\{R, d_1, d_2, \theta_1, \theta_2, \chi\}$. For explicit definition of the latter

coordinates and the reduced masses μ_1, μ_2, μ_R attributed to the internal vectors $\mathbf{d}_1, \mathbf{d}_2, \mathbf{R}$, see Ref. 41. Since $\sin\theta_2 \rightarrow$ small for the CHNO family, we obtain

$$\theta_1 \rightarrow 90^\circ \quad A \rightarrow \hbar^2/2\mu_1 d_1^2 = B(d_1) = B(\mathrm{HX}) \tag{9}$$

and

$$\theta_1 \rightarrow 180^\circ, \quad A \rightarrow 1/\mathrm{small} = \mathrm{large}, \tag{10}$$

assuming $A \approx \hbar^2/2I_{zz}$, where B(HX) is the rotational constant of the HX subunit in the (diatom+diatom) orthogonal description. Note that the latter results, explaining the behavior of A_{opt} seen in Fig. 7(a), are valid for any HXYZ molecule with a nearly linear XYZ subunit. In a similar fashion, one may analyze also Fig. 7(b), where the finite value of A_{opt} at $\angle(\mathrm{XYZ}) = 180°$ is due to $\angle(\mathrm{HXY})_{\mathrm{opt}} \neq 180°$ for the optimum hockey-stick structure of HNCO, HOCN, HONC, and HCCN.

Equations (9) and (10) are obtained from I_{zz} of Eq. (8), valid for the orthogonal description of tetratomic molecules. It is easy to verify that similar results may be derived also from the moment of inertia I_{zz} given by

$$MI_{zz} = m_H m_{\mathrm{XYZ}} r_{12}^2 \sin^2\alpha + m_{\mathrm{HXY}} m_Z r_{34}^2 \sin^2\beta + 2m_H m_Z r_{12} r_{34} \sin\alpha \sin\beta \tag{11}$$

for a HXYZ molecule in the bond-distance-bond-angle formulation with the z axis aligned with r(XY). In Eq. (11), $\alpha = \angle(\mathrm{HXY})$ and $\beta = \angle(\mathrm{XYZ})$, whereas $m_{ij} = m_i + m_j$, $m_{ijk} = m_{ij} + m_k$, and $M = \Sigma m_i$ for $1 = H$, $2 = X$, $3 = Y$, and $4 = Z$, such that $r_{12} = r(\mathrm{HX})$ and $r_{34} = r(\mathrm{YZ})$.

B. Rovibrational behavior

In the body-fixed formalism introduced in Ref. 41, the body-fixed z axis is aligned with the internal vector $\mathbf{R}$, whereas the body-fixed $z \wedge x$ plane is defined by $\mathbf{R}$ and $\mathbf{d_1}$, such that θ_1 is the angle between $\mathbf{R}$ and $\mathbf{d_1}$. The orbiting of the vector $\mathbf{d_2}$ is then described by the polar angle θ_2 and azimuthal angle χ. We recall that the kinetic energy contribution for the orthogonal description of the internal molecular geometry in the body-fixed formulation of the rovibrational motion is given by

$$2T_{\theta_1} = -\hbar^2 f(d_1, R)\left[\partial_{\theta_1}^2 + \cot\theta_1 \partial_{\theta_1} + \frac{(\partial_\psi - \partial_\chi)^2}{\sin^2\theta_1}\right] \tag{12}$$

for the bending angle θ_1 and by

$$2T_{\theta_2} = -\hbar^2 f(d_2, R)\left[\partial_{\theta_2}^2 + \cot\theta_2 \partial_{\theta_2} + \frac{\partial_\chi^2}{\sin^2\theta_2}\right] \tag{13}$$

for the bending angle θ_2, where ∂_α stands for $\partial/\partial\alpha$ and ∂_α^2 for $\partial^2/\partial\alpha^2$. The third Euler angle ψ defines rotation about the body-fixed z axis. The inverse of the reduced mass for the bending coordinate θ_i reads

$$f(d_i, R) = 1/\mu_i d_i^2 + 1/\mu_R R^2 \tag{14}$$

for $i = 1, 2$. Inspection of Eqs. (12) and (13) clearly emphasizes two features which are relevant for the rovibrational behavior of tetratomic molecules.

The out-of-plane (torsional) motion may influence the bending vibration associated with θ_2, as seen in Eq. (13). This effect is particularly strong in the case of an angular potential independent of the torsional angle χ, when a vibrational angular momentum l may arise. In the small-amplitude limit around $\theta_2 = 0, 180°$ assuming $V \neq V(\chi)$, a Taylor expansion of the kinetic energy contribution of Eq. (13) in combination with the harmonic potential energy in θ_2 gives the Hamiltonian of the two-dimensional isotropic oscillator,

$$2H_{2D} = -\hbar^2 f(d_2, R)\left(\partial_{\theta_2}^2 + \frac{\partial_{\theta_2}}{\theta_2} + \frac{\partial_\chi^2}{\theta_2^2}\right) + k_2\theta_2^2, \tag{15}$$

with the volume element $\theta_2 d\theta_2$ and eigenvalues $E_{n,l} = \hbar\omega(n+1) = \hbar\omega(2n_r + |l| + 1)$, where l is the vibrational angular momentum quantum number, for which $l = n, n-2, \ldots, -n+2, -n$ holds.

In view of a shallow torsional well in Fig. 4 and a low-energy optimum hockey-stick structure of Fig. 3, the onset of the two-dimensional oscillatorlike structure is to be expected already at low energies for the (small-amplitude) heavy atom bending XYZ vibration in combination with the torsion (out-of-plane motion) for HNCO, HOCN, and HONC. In other words, clustering of the ν_5 and ν_6 rovibrational states is to be expected in the bent molecule limit. One may also note that the harmonic ω(XYZ) wavenumber is by 50–60 cm^{-1} smaller than the harmonic torsional wavenumber for HNCO, HOCN, and HONC, as seen in Table III of the present work and Table VII of Ref. 23.

We now consider Eq. (12) which gives the kinetic energy of the in-plane bending vibration along θ_1. Intrinsic kinetic energy coupling always exists between θ_1- and a-type rotation (described by the angle ψ, such that $\hat{L}_z = -\imath\hbar\partial_\psi$) and between θ_1 and the vibrational angular momentum (described by the angle χ, such that $\hat{l}_z = -\imath\hbar\partial_\chi$). Note that the latter statement is also valid for n-atomic molecules, when the overall vibrational angular momentum $\hat{l}$ is given by a sum $\hat{l} = \hat{l}_2 + \cdots + \hat{l}_{n-2}$ of $n-3$ contributions.[41]

To rationalize the kinetic coupling involving θ_1, we first recall that the overall (total) molecular rotation of an n-atomic molecule is given by[42]

$$\hat{J} = \hat{l}_R + \hat{l}_1 + \hat{l}_2 + \cdots + \hat{l}_{n-2} \tag{16}$$

in the space fixed reference frame with the origin in the molecular center of mass, where $\hat{l}_i$ is the angular momentum associated with the ith internal vector. In the latter expression, the convention introduced in Ref. 41 is employed, where $\mathbf{R}$ denotes the internal vector chosen for the global axis formulation.[42] To make the total rotation explicit in the kinetic energy expression, we write

$$\hat{l}_R = \hat{J} - (\hat{l}_1 + \hat{l}_2 + \ldots + \hat{l}_{n-2}), \tag{17}$$

thereby eliminating one of the angular momentum operators, e.g., $\hat{l}_R$, from the kinetic energy expression. In practice, the internal vector $\mathbf{R}$ in the global axis description specifies the orientation of the body-fixed z axis, providing two Euler angles. The third Euler angle ψ is then introduced with the help of the internal vector $\mathbf{d}_1$, such that $\mathbf{R} \wedge \mathbf{d_1}$ defines the

body-fixed $z \wedge x$ plane. In the resulting body-fixed frame, the motion of the internal vectors $\mathbf{d}_i$ for $i=2,\ldots,n-2$ is given by means of the usual spherical polar angles θ_i and χ_i, describing the in-plane bending motion involving $\mathbf{R}$, $\mathbf{d}_i$ and the out-of-plane motion involving $\mathbf{R}$, $\mathbf{d}_1$, $\mathbf{d}_i$, respectively, whereas the in-plane bending motion involving $\mathbf{R}$, $\mathbf{d}_1$ is described by θ_1. In total, there are, thus, $n-2$ bending angles and $n-3$ torsional angles, in addition to $n-1$ radial degrees of freedom.

Since $\hat{\mathbf{l}}_{R,z}=0$ also holds, as given by Eq. (25) of Ref. 43, we further have

$$\hat{l}_{1,z} = \hat{J}_z - (\hat{l}_{2,z} + \cdots + \hat{l}_{n-2,z}). \tag{18}$$

The latter condition may be termed a "body-fixed constraint," affecting solely the bending motion between $\mathbf{R}$ and $\mathbf{d}_1$, as easily seen in Eq. (12) for tetratomic molecules. In other words, the motion correlated with the internal vector $\mathbf{d}_1$ specifying the body-fixed reference $z \wedge x$ plane may establish some sort of a bridge between the pure vibrational and pure rotational motion of polyatomic molecules. However, it may also cause mixing of vibrational and rotational features. This is the case whenever the linearity region in θ_1 assumes an important role in the overall internal dynamics, such that the motion in θ_1 has to be treated together with both the a rotation and torsion (overall vibrational angular momentum) due to a singular term in θ_1 in Eq. (12).

The rovibrational energy pattern associated with the in-plane θ_1 bending motion depends on the potential energy properties, such as the HXY MEPs of Fig. 2, and the kinetic energy properties, such as the bending reduced mass of Eq. (14), and kinetic energy coupling of θ_1 with the a rotation and vibrational angular momentum, as given by Eq. (12). For $\theta_1^e=0,180°$ at equilibrium, the rovibrational pattern associated with θ_1 is of a two-dimensional oscillator type, leading to an overall linear-molecule pattern whenever the optimum hockey-stick structure in (θ_2,χ) occurs at low energy. This is the case for fulminic acid, found to possess a linear equilibrium structure in the present work.

In a first approximation, the CHNO isomers may be considered as systems with a strictly linear heavy atom XYZ skeleton, allowing to simulate their rovibrational behavior as that of triatomic molecules. Under these circumstances, the rovibrational energy structure will depend only on the optimum barrier to linearity, Fig. 2, and the optimum rotational constant A_{opt}, Fig. 7. The onset of the linear-molecule pattern will ultimately occur also for the three nonlinear CHNO isomers, however, at different energy scales. The influence of angular momentum conservation on the bending HXY (i.e., θ_1) vibration in the intermediate transition region, as well as the effects due to Coriolis (c-type) and l-type coupling, Fig. 6, and due to the anharmonicity, Fig. 2, clearly call for particular attention in the full-dimensional approach to the internal dynamics of HNCO, HOCN, HCNO, and HONC. These observations will be investigated in more detail in our future work, employing a numerical approach suitable for efficient and accurate full-dimensional calculation of rovibrational energy levels of general tetratomic molecules.[41,44]

The use of an orthogonal description of the rovibrational motion in the preceding discussion merits some remarks: This representation does not restrict the generality of the argument because it contains singularity terms of the highest possible order and clearly identifies the dominant quadratic contributions. At the same time it actually simplifies computational approaches. A full discussion and comparison of the kinetic energy operators for general polyatomic molecules in the orthogonal and nonorthogonal formulations can be found in Ref. 43. Although the reference system should be immaterial for the construction of suitable vibrational coordinates, the common concepts of vibrational coordinates (based on the commonly used spherical polar parametrization) make an implicit assumption about the underlying axis system.[42] An explicit formulation of the reference axis frame helps to understand the relevant physics of the vibrational mode, bridging the concepts of vibrational coordinates and of rotational coordinates, which may additionally lead to a behavior usually termed *quasilinear*.

VI. CONCLUSION

In the present work, we have extended our study of the CHNO system by a detailed analysis of isofulminic acid. We have employed coupled-cluster theory at the CCSD(T) level in combination with large basis sets to determine the equilibrium structure of HONC. The latter structure was calculated to be planar and bent, with a heavy atom ONC bond angle departing from linearity by 7.5°. Several extrapolation strategies were used in our attempt to access the CBS limit for the geometrical parameters, the absolute energy, and the height of the barrier to linearity. We have also demonstrated the importance of including diffuse functions into the standard correlation consistent bases to obtain converged molecular structures for the four most stable members of the CHNO isomer family. It is shown that augmented basis functions improve basis set convergence and affect the barriers to linearity (up to 120 cm^{-1}) and the energetics (up to 50 cm^{-1}). Our results should provide the most accurate theoretical estimates to date for the equilibrium geometries of HNCO, HOCN, HCNO, and HONC.

Our investigation of the singly augmented aug-cc-p(C)VXZ and doubly augmented d-aug-cc-pVXZ correlation consistent sets of basis functions provides a solid ground for the calculations of electric properties, such as dipole moments and nuclear quadrupole coupling constants, which are useful to molecular spectroscopists. The reason for this is that the basis sets studied here ensure a proper description of both core and valence electrons, a key feature necessary to obtain reliable results for electric field gradients. In our work in progress, electric, magnetic, and spectroscopic properties of the CHNO family are currently under investigation. As a part of the latter study, we may already now announce the first gas phase detection of isofulminic acid by means of microwave spectroscopy,[22] guided by our *ab initio* results some of which are reported in the present work.

Optimum potential energy paths in the direction of the HXY and XYZ coordinates were additionally studied. The MEPs along the bond angle involving hydrogen were determined to be strongly anharmonic, with barriers to linearity of

1839 cm^{-1} for HNCO, 9406 cm^{-1} for HOCN, and 16 761 cm^{-1} for HONC in the CCSD(T)/aug-cc-pCVQZ approach. On the other hand, straightening of the heavy atom chain involves small barriers of only 339, 31, and 56 cm^{-1} for HNCO, HOCN, and HONC, respectively. For fulminic acid, HCNO, the linear equilibrium geometry is found at the CCSD(T)/aug-cc-pCVQZ level. Possible implications for the rovibrational and spectroscopic behavior of the CHNO isomers are analyzed combining the optimum angular MEPs with dominant kinetic energy contributions. It is found that the large-amplitude hydrogen bending vibration and the small-amplitude skeletal (heavy atom) bending vibration exhibit different energy patterns. In addition, these zero-order solutions may account for the majority of spectroscopic properties relevant for quasilinear systems, in agreement with the conclusion of Neely[45] that "the large centrifugal distortion is not really an anomalous effect but is a direct consequence of strong coupling between the in-plane bending vibration with the rotation about the axis of the least moment of inertia." Further theoretical studies for the CHNO isomer family based on full-dimensional calculations for the rovibrational energies are part of our ongoing work.

ACKNOWLEDGMENTS

Access to the high performance computers of the Institut du Développement et des Ressources en Informatique Scientifique (IDRIS) through Grant No. 82170 is gratefully acknowledged.

[1] K. Yamada and M. Winnewisser, Z. Naturforsch. A **31**, 139 (1976).
[2] B. P. Winnewisser, in *Molecular Spectroscopy: Modern Research*, edited by K. N. Rao (Academic, Orlando, 1985), Vol. 3, p. 321.
[3] M. Mladenović, P. Botschwina, and C. Puzzarini, J. Phys. Chem. **110**, 5520 (2006).
[4] N. Pinnavaia, M. J. Bramley, M.-D. Su, W. H. Green, and N. C. Handy, Mol. Phys. **78**, 319 (1993).
[5] J. H. Teles, G. Maier, B. A. Hess, Jr., L. J. Schaad, M. Winnewisser, and B. P. Winnewisser, Chem. Ber. **122**, 753 (1989).
[6] D. Poppinger, L. Radom, and J. A. Pople, J. Am. Chem. Soc. **99**, 7806 (1977).
[7] A. D. McLean, G. H. Loew, and D. S. Berkowitz, J. Mol. Spectrosc. **64**, 184 (1977).
[8] M. S. Schuurman, S. R. Muir, W. D. Allen, and H. F. Schaefer III, J. Chem. Phys. **120**, 11586 (2004).
[9] M. E. Jacox and D. E. Milligan, J. Chem. Phys. **40**, 2457 (1964).
[10] V. E. Bondybey, J. H. English, C. W. Mathews, and R. J. Contolini, J. Mol. Spectrosc. **92**, 431 (1982).
[11] G. Maier, J. H. Teles, B. A. Hess, Jr., and L. J. Schaad, Angew. Chem., Int. Ed. Engl. **27**, 938 (1988).
[12] G. Maier, A. Bothur, J. Eckwert, H. P. Reisenauer, and T. Stumpf, Liebigs Ann. **1997**, 2505.
[13] B. P. Winnewisser, M. Winnewisser, and F. Winther, J. Mol. Spectrosc. **51**, 65 (1974).
[14] E. L. Ferretti and K. N. Rao, J. Mol. Spectrosc. **51**, 97 (1974).
[15] K. Yamada, B. P. Winnewisser, and M. Winnewisser, J. Mol. Spectrosc. **56**, 449 (1975).
[16] B. P. Winnewisser and P. Jensen, J. Mol. Spectrosc. **101**, 408 (1983).
[17] M. Niedenhoff, K. M. T. Yamada, M. Winnewisser, and S. C. Ross, J. Mol. Struct. **352-353**, 423 (1995).
[18] S. Albert, M. Winnewisser, and B. P. Winnewisser, Ber. Bunsenges. Phys. Chem. **100**, 1876 (1996).
[19] S. Albert, K. K. Albert, M. Winnewisser, and B. P. Winnewisser, J. Mol. Spectrosc. **599**, 347 (2001).
[20] M. C. McCarthy, W. Chen, M. J. Travers, and P. Thaddeus, Astrophys. J. **129**, 611 (2000).
[21] S. Brünken, C. A. Gottlieb, M. C. McCarthy, and P. Thaddeus, Astrophys. J. (in press).
[22] M. Mladenović, M. Lewerenz, M. C. McCarthy, and P. Thaddeus (unpublished).
[23] M. Mladenović and M. Lewerenz, Chem. Phys. **343**, 129 (2008).
[24] A. M. Mebel, A. Luna, M. C. Lin, and K. Morokuma, J. Chem. Phys. **105**, 6439 (1996).
[25] M. Winnewisser, B. P. Winnewisser, I. R. Medvedev, F. C. De Lucia, S. C. Ross, and L. M. Bates, J. Mol. Struct. **798**, 1 (2006).
[26] C. Hampel, K. A. Peterson, and H.-J. Werner, Chem. Phys. Lett. **190**, 1 (1992) (and references therein).
[27] M. J. O. Deegan and P. J. Knowles, Chem. Phys. Lett. **227**, 321 (1994).
[28] T. H. Dunning, Jr., J. Chem. Phys. **90**, 1007 (1989).
[29] D. E. Woon and T. H. Dunning, Jr., J. Chem. Phys. **103**, 4572 (1995).
[30] R. A. Kendall, T. H. Dunning, and R. J. Harrison, J. Chem. Phys. **96**, 6796 (1992).
[31] M. Mladenović, M. Lewerenz, P. Rosmus, G. Cilpa, and G. Chambaud, Chem. Phys. **346**, 237 (2008).
[32] T. J. Lee and P. R. Taylor, Int. J. Quantum Chem., Symp. **23**, 199 (1989).
[33] H.-J. Werner, P. J. Knowles, R. Lindh *et al.*, MOLPRO, version 2006.1, a package of *ab initio* programs, see http://www.molpro.net.
[34] I. Mills, T. Cvitaš, K. Homann, N. Kallay, and K. Kuchitsu, *Quantities, Units and Symbols in Physical Chemistry*, 2nd ed. (Blackwell, Oxford, 1993).
[35] T. Helgaker, W. Klopper, H. Koch, and J. Noga, J. Chem. Phys. **106**, 9639 (1997).
[36] P. R. Bunker, B. M. Landsberg, and B. P. Winnewisser, J. Mol. Spectrosc. **74**, 9 (1979).
[37] A. L. L. East, C. S. Johnson, and W. D. Allen, J. Chem. Phys. **98**, 1299 (1993).
[38] A. V. Lapinov, G. Y. Golubiatnikov, V. N. Markov, and A. Guarnieri, Astron. Lett. **33**, 121 (2007).
[39] Note a misprint in Eq. (28) of Ref. 40, where I_{zx} should read $I_{zx}/\mu = d_{1s}^2 \sin\theta_1 \cos\theta_1 + d_{2s}^2 \sin\theta_2 \cos\theta_2 \cos\chi$ in terms of the mass-scaled coordinates d_{1s} and d_{2s} used there.
[40] M. Mladenović, Spectrochim. Acta, Part A **58**, 795 (2002).
[41] M. Mladenović, J. Chem. Phys. **112**, 1070 (2000).
[42] M. Mladenović, J. Chem. Phys. **113**, 10524 (2000).
[43] M. Mladenović, J. Chem. Phys. **112**, 1082 (2000).
[44] M. Mladenović, in NIC Symposium 2001, Jülich, 2002, edited by H. Rollnik and D. Wolf, Vol. 9, p. 85.
[45] G. O. Neely, J. Mol. Spectrosc. **27**, 177 (1968).